Hindawi
International Journal of Aerospace Engineering
Volume 2019, Article ID 8916303, 11 pages
https://doi.org/10.1155/2019/8916303

Research Article

Influence of the Decelerator Grid on the Optical Performance of the Ion Thruster

Chang Lu[1,2] **Yide Zhao**[2] **Jie Wan**[3] **Yuchuan Chu**[4] **Liang Zheng**[5] **and Yong Cao**[1]

[1]*School of Mechanical Engineering and Automation, Harbin Institute of Technology, Shenzhen, 518055 Shenzhen, China*
[2]*Lanzhou Institute of Space Technology Physics, 730000 Lanzhou, China*
[3]*Fundamental Space Science Research Center, Harbin Institute of Technology, Harbin 150001, Heilongjiang, China*
[4]*School of Mechanical Engineering, Dongguan University of Technology, 523808 Dongguan, China*
[5]*School of Science, Harbin Institute of Technology, Shenzhen, 518055 Shenzhen, China*

Correspondence should be addressed to Yuchuan Chu; ychuan.chu@dgut.edu.cn and Yong Cao; yongc@hit.edu.cn

Received 28 September 2018; Revised 6 December 2018; Accepted 14 January 2019; Published 7 May 2019

Academic Editor: Marco Pizzarelli

In order to reduce the erosion of the ion thruster accelerator grid, which is caused by charge-exchange (CEX) ions, the 2-grid optical system is added to a decelerator grid to block the reflux CEX ions. The previous experiment and simulation results have proven that the decelerator grid can effectively reduce the Pit and Groove erosion. However, the influence of the decelerator grid on the optical performance has not yet been studied well. In this paper, a three-dimensional Immersed Finite Element Method-Particle in Cell-Monte Carlo Collision (IFE-PIC-MCC) algorithm was adopted to investigate the effect of the decelerator grid on the optical performance under crossover and normal circumstances. Results show that the decelerator grid has no effect on the focusing state and the distribution of beam ions. It also has little effect on the CEX ions from the upstream and extraction (center) regions. However, it has great influence on the downstream CEX ions. When the upstream plasma number density is small, the decelerator grid will cause most of the downstream reflux CEX ions to impinge on the accelerator grid aperture barrel, resulting in the significant increase of the Barrel erosion of the accelerator grid. With the increase of the upstream plasma number density, the downstream reflux CEX ions tend to impact the downstream surface of the decelerator grid, which means the decelerator grid begins to block the downstream backflow of CEX ions.

1. Introduction

The failure of the accelerator grid structure is mainly caused by the sputtering of the charge-exchange (CEX) ions, which erodes the downstream surface and the apertures of the accelerator. The erosion of the accelerator grid can be divided into two types: Pit and Groove erosion and Barrel erosion. In order to prevent the accelerator structural failure caused by the Pit and Groove erosion, a decelerator grid is introduced to the classical 2-grid optical system. Many ion thruster tests have shown that the decelerator grid can significantly reduce the Pit and Groove erosion [1–3]. However, the effects of the decelerator grid on the optical system, such as on the extraction process of beam ions and CEX ions, have not been fully studied. The performance of the thrust is determined by the extraction capability of the optical system, and the extraction characteristics of the optical system on the CEX ions determine its service life. Therefore, it is crucial to investigate the influence of the decelerator grid on the optical system in order to provide theoretical guidance on the optimal design of the optical system and ultimately prolong the service life of the optical system.

The influence of the decelerator grid on the optical system can be investigated by experimental tests and numerical simulations. Compared to the experimental method, the numerical simulation method is not only cost-efficient but can also avoid the influence of irrelevant variables to the object. Hence, currently, a series of numerical studies have been developed to study the grid erosion. For example, numerical simulation models have been developed by the

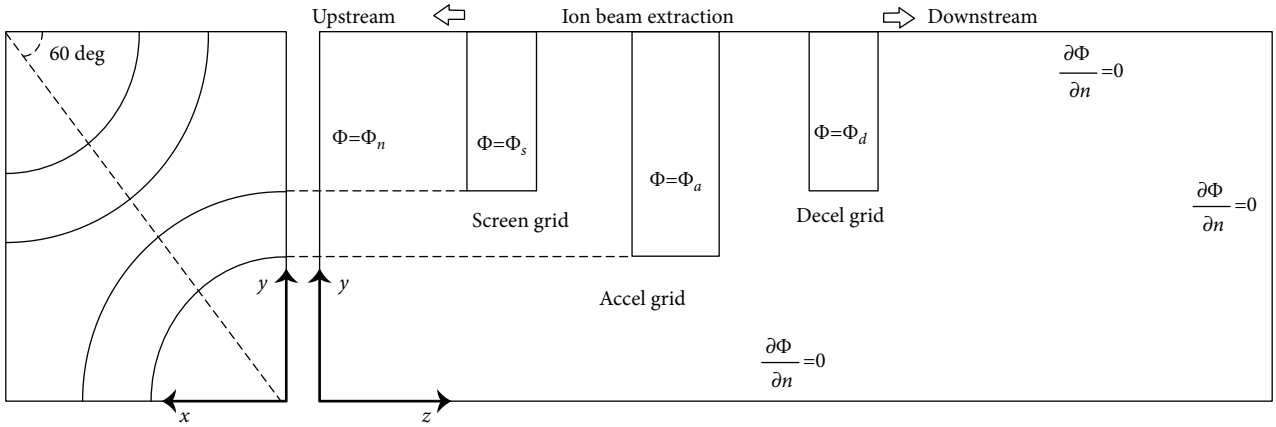

Figure 1: Two-quarter aperture numerical simulation model.

Jet Propulsion Laboratory to investigate the processes which limit the life of the accelerator grid [4, 5]. Anbang et al. [6] use the Particle in Cell-Monte Carlo Collision (PIC-MCC) method to simulate the ion dynamics and charge-exchange processes in a 3-grid system. Wirz et al. [2] study the accelerator grid erosion of a xenon-ion propulsion system (XIPS) ion thruster and find that the decelerator grid effectively reduces the accelerator grid Pit and Groove erosion by blocking the backflow of downstream CEX ions. Wang et al. [4] adopt a fully 3-D particle simulation model to study the plasma flow and downstream face erosion of the NASA Solar Technology Application Readiness (NSTAR) ion thruster optics. Kafafy and Wang [7–11] study the dynamic behavior of beam ions in ion optics and the interactions between nonuniform plasmas and complex objects. Cao et al. [12], Jian et al. [13], and Lu et al. [14] study the Barrel erosion mechanism of the NSTAR ion thruster accelerator grid and the influence of background pressure on the impact current of the accelerator grid by the Immersed Finite Element Method-Particle in Cell-Monte Carlo Collision (IFE-PIC-MCC) algorithm.

However, most of the previous studies are based on the assumptions that the upstream plasma number density has a uniform distribution; the influence of the change in operation conditions on the distribution characteristics of beam ions and CEX ions in the 3-grid system is not considered. Hence, in this paper, the influence of the decelerator grid on the optical performance under different operation conditions is investigated. In the second section, the parameters of the 3-grid system, the simulation domain, and other numerical simulation settings are briefly introduced. The third section compares the performance of the 2-grid optics and the 3-grid optics under two circumstances considering or without considering the CEX ions, including the focusing curves, the ion extraction capabilities, and the accelerator grid erosion of these two optics. The fourth section presents the conclusions of this paper.

2. Numerical Simulation Setup

Referring to Refs. [15–18], it can be found that, for a basic 3-grid ion extraction system, the decelerator grid is normally slightly thinner than the screen grid, and its apertures are usually slightly larger than or equal to the screen grid's apertures. The gap between the accelerator grid and the decelerator grid is usually the same with the distance between the screen grid and the accelerator grid.

In this paper, a prototype of a 3-grid system was constructed. The geometric parameters of the screen grid and accelerator grid are based on those of the NSTAR 2-grid optical system [4], but their voltages are different from the NSTAR 2-grid optical system. The decelerator grid was designed based on the principles stated in Refs. [15–18]. The size and spacing of the decelerator grid hole are the same as those of the screen grid; the distance between the decelerator grid and the accelerator grid is equal to that between the screen and accelerator grids. The thickness of the decelerator grid is designed to be the same as that of the screen grid. In addition, in the simulation, the parameters of the screen and accelerator grids of the 2-grid system are exactly the same with those of the 3-grid system.

Figure 1 presents the two-quarter aperture numerical simulation model used in this paper. The computational domain is a 3-D rectangle with two-quarter apertures. The Dirichlet potential boundary condition is adopted on the upstream surface, and the other surfaces satisfy the Neumann boundary condition. When the particles collide with the $z = 0$ and $z = z_{\max}$ surfaces, they are absorbed, whereas those that hit the other four surfaces are reflected.

In Figure 2, the CEX ion generation region is divided into four regions:

(1) *Upstream region:* the upstream boundary of the simulation domain to the upstream surface of the screen grid

(2) *Extraction (center) region:* for the 2-grid system, the extraction (center) region is from the upstream surface of the screen grid to the downstream surface of the accelerator grid where the center hole is located; for the 3-grid system, the extraction (center) region is from the upstream surface of the screen grid to the downstream surface of the decelerator grid where the center hole is located

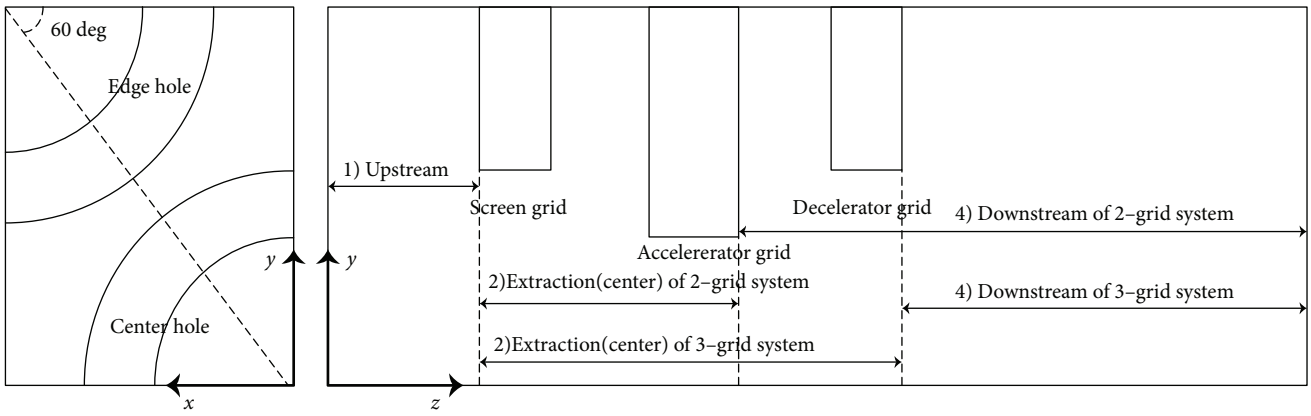

Figure 2: The CEX ion generation region division.

(3) *Extraction (edge) region:* for the 2-grid system, the extraction (edge) region is from the upstream surface of the screen grid to the downstream surface of the accelerator grid where the edge hole is located; for the 3-grid system, the extraction(edge) region is from the upstream surface of the screen grid to the downstream surface of the decelerator grid where the edge hole is located

(4) *Downstream region:* for the 2-grid system, the downstream region is from the downstream surface of the accelerator grid to the downstream boundary of the simulation domain; for the 3-grid system, the downstream region is from the downstream surface of the decelerator grid to the downstream boundary of the simulation domain

In addition, the material of the optics system is molybdenum and the propellant is xenon. The normalized geometric dimensions for the ion optic model are given in Table 1, and Table 2 summarizes the operating conditions for the numerical simulations.

According to the upstream plasma number density, a set of meshes are selected and one of these meshes is suited for a range of upstream plasma number densities, as shown in Table 3.

The simulation method, as well as the procedures for calculating the beam ion, neutral atom, and CEX ion, and the prediction of the accelerator grid Barrel erosion can be referred to Ref. [12].

Table 1: Normalized geometric parameters [12].

Geometric parameters	Normalized
Screen hole diameter (d_s)	43.85
Screen grid thickness (t_s)	9
Acceleration hole diameter (d_a)	26.56
Acceleration grid thickness (t_a)	19
Screen-to-acceleration-grid gap (l_g)	15
Center-to-center hole spacing (l_{cc})	50.87

Table 2: Normalized operating conditions for the ion optics [12].

Voltage parameters	Normalized
Net acceleration (V_N)	360
Screen grid voltage (V_s)	354
Accelerator grid voltage (V_a)	-38
Decelerator grid voltage (V_d)	0

Table 3: Meshing parameters used in the simulations.

Density	Mesh length	
	Δ_z	$n_x \times n_y \times n_z$
$n_0 \le 1.0$	5.2566×10^{-5}	$27 \times 27 \times 281$
$1.0 < n_0 \le 2.0$	2.6283×10^{-5}	$53 \times 53 \times 401$

3. Simulation Results and Discussion

3.1. Comparison of the 2- and 3-Grid Optical System Performance

3.1.1. Without CEX Ions. Table 4 shows the beam current per hole J_b, the impingement current of the accelerator grid per hole J_a, and the ratio between them without considering CEX ions. After adding the decelerator grid, the beam current of the 3-grid system is almost the same with that of the 2-grid system, and the impingement current of the accelerator grid and the ratio is basically the same as well. Also, the cross limit for these two optics is still at $n_0 = 0.2$.

Hence, the working conditions of these two types of optics can be divided into the over-focused condition and the normal-focused condition according to the impingement current of the accelerator grid. When $n_0 \le 0.2$, the impingement current of the accelerator grid is greater than 0 and the optics is under the over-focused condition; when $n_0 \ge 0.2$, it is equal to 0 and the optics is under the normal-focused condition.

Figures 3 and 4 illustrate the characteristics of the beam ion under the above two focusing states, respectively, and Figures 5 and 6 are the corresponding potential distributions.

Table 4: Ratio of the impingement current of the accelerator grid to the beam current without CEX ions.

Density	J_b (μA)		J_a (μA)		J_a/J_b (%)	
	2-grid	3-grid	2-grid	3-grid	2-grid	3-grid
0.05	7.8349	7.8348	0.1211	0.1277	1.5455	1.6304
0.075	11.8554	11.8585	0.1255	0.1282	1.0587	1.0808
0.15	24.2087	24.2102	0.0354	0.0360	0.1460	0.1487
0.2	32.2510	32.2554	0.0055	0.0064	0.0166	0.0199
0.25	38.5102	38.5018	0.0001	0.0000	0.0000	0.0000
0.5	79.3658	78.0667	0.0000	0.0000	0.0000	0.0000
0.75	113.9897	110.8854	0.0000	0.0000	0.0000	0.0000
1.0	147.5525	146.1607	0.0000	0.0000	0.0000	0.0000
1.5	189.3685	189.2688	0.0000	0.0000	0.0000	0.0000
2.0	271.9309	271.9175	0.0000	0.0000	0.0000	0.0000

By comparing Figures 3–6, it is found that, after adding the decelerator grid, the beam ion distribution and the upstream sheath structure are basically unchanged. The decelerator grid mainly changes the potential structure downstream of the accelerator grid. Because the focusing characteristics of the beam ion are determined by the potential structure of the upstream sheath, the impingement current of the accelerator grid of the 3-grid optics, the ratio of the beam current to the impingement current of the accelerator grid, and the crossing limit of the 3-grid optics are basically the same with those of the 2-grid optics.

3.1.2. With CEX Ions. Figure 7 illustrates the distribution of neutral atoms at $n_0 = 0.5$. In the 3-grid optics, the distribution of neutral atoms changes little compared with the 2-grid optics. The obvious change is that the atom density near the downstream of the accelerator grid in the 3-grid optics is slightly increased, which is caused by the throttling of the decelerator grid. In the following simulation results, the number density of atoms used in the calculation of CEX ions in the 2-grid optics and the 3-grid optics is assumed to increase linearly with the increase of the upstream plasma number density according to the ratio of the upstream plasma number density to $n_0 = 0.5$. For instance, at $n_0 = 0.075$, the density of neutral atoms will be reduced by 0.15 times, while the density of neutral atoms will be 4 times of that at $n_0 = 0.5$.

The distributions of beam ions and CEX ions in the two types of optics at $n_0 = 0.075$ and $n_0 = 2.0$ are shown in Figures 8 and 9, respectively. Since the number density of the CEX ion is much smaller than that of the beam ion, the potential distribution is the same with that without the CEX ion. And it can be found that the CEX ions downstream of the accelerator grid decrease in the 3-grid optics because the decelerator grid blocks a large number of backflow CEX ions. Figure 10 presents the ratio of the impingement current of the accelerator grid to the beam current while considering CEX ions. It can be seen that, as the decelerator grid blocks many backflow CEX ions, the ratio of the 3-gird optics is significantly reduced.

3.2. Effect of the Decelerator Grid on the Accelerator Grid Erosion Induced by CEX Ions. Because the decelerator grid has a significant impact on the downstream CEX ions, and the erosion of the accelerator grid is largely caused by the downstream CEX ions, in this section, the accelerator gird erosion caused by CEX ions in the 2-grid system and the 3-grid system is compared. In the estimation of the accelerator grid erosion, the erosion calculation is based on the distribution of CEX ions and the potential in steady state without considering the effect of aperture enlargement of the accelerator grid.

In Table 5, the average erosion rates of the Barrel erosion and Pit and Groove erosion under four different upstream plasma number densities of the 2-grid and 3-grid optics are compared. Under these four conditions, the Pit and Groove erosion rate of the accelerator grid of the 3-grid optical system all decreased significantly, comparing with the 2-grid optical system. However, comparing with the 2-grid optical system, the Barrel erosion rate of the 3-grid optical system was increased significantly only at the first three operating conditions (except at $n_0 = 2.0$). Furthermore, it can also be seen that the influence of the decelerator grid on the accelerator grid Barrel erosion changes with the variation of working conditions. In addition, the average erosion rate of the accelerator grid Barrel erosion in the 3-grid optics is at least one order of magnitude higher than that of the Pit and Groove erosion, so the accelerator gird Barrel erosion becomes a more important factor affecting the life of the 3-grid optics.

Tables 6–9 compare the impingement current of the accelerator grid and the average impingement energies of CEX ions from four different regions under the above four operating conditions (that is, $n_0 = 0.075$, $n_0 = 0.2$, $n_0 = 0.75$, and $n_0 = 2.0$). It can be found that the impingement current caused by the CEX ions from upstream and extraction (center) regions is basically unchanged and the impingement current of the accelerator grid caused by the CEX ion from the extraction (edge) region decreases under all of these conditions. However, the impingement current of CEX ions from downstream increases significantly at $n_0 = 0.075$, $n_0 = 0.2$, and $n_0 = 0.75$ but decreases slightly at $n_0 = 2.0$. In addition, the change of the impingement energy of CEX ions from these four regions is not evident after adding the decelerator grid.

For the 2-grid optics, at $n_0 = 0.075$ and $n_0 = 0.2$, the CEX ions from upstream lead to not only the greatest impingement current of the accelerator grid but also the largest impingement energy, so the main cause of the accelerator Barrel erosion is the CEX ions from the upstream. However, for the 3-grid optics, the impingement current of the accelerator grid and the impingement energy of CEX ions from upstream are basically unchanged, but the CEX ion impingement current of the accelerator grid from downstream increases significantly to an order of magnitude. Hence, CEX ions from downstream are also the main factor causing the accelerator grid Barrel erosion. Therefore, after adding the decelerator grid, the accelerator grid Barrel erosion increases significantly at $n_0 = 0.075$ and $n_0 = 0.2$.

At $n_0 = 0.75$, in the 2-grid optics, although there are still CEX ions from the upstream impinging on the accelerator

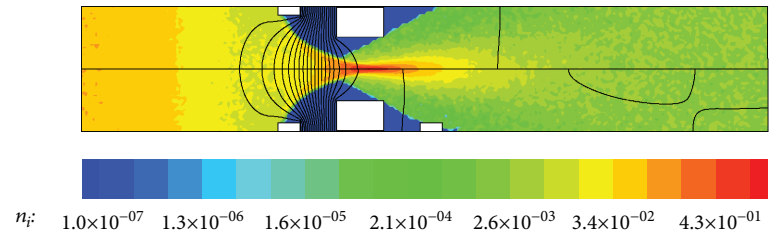

Figure 3: Beam distribution without CEX ($n_0 = 0.075$).

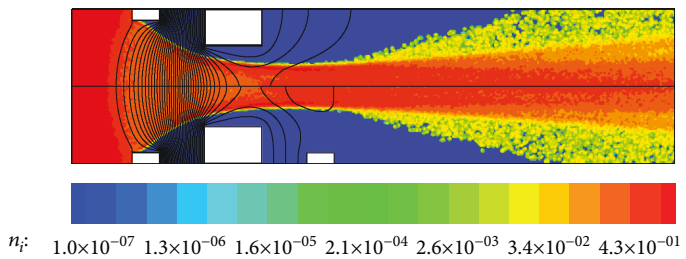

Figure 4: Beam distribution without CEX ($n_0 = 2.0$).

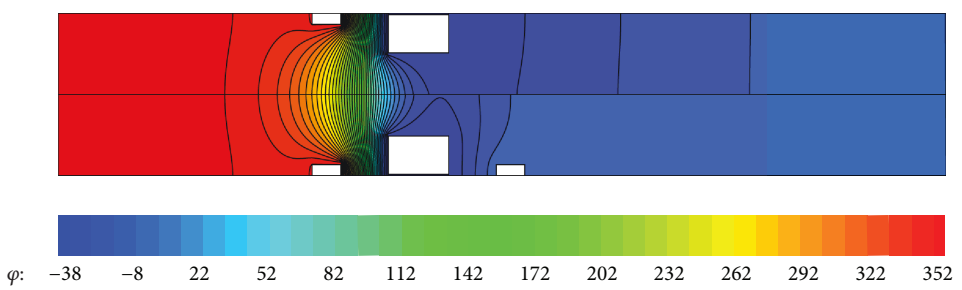

Figure 5: Potential distribution ($n_0 = 0.075$).

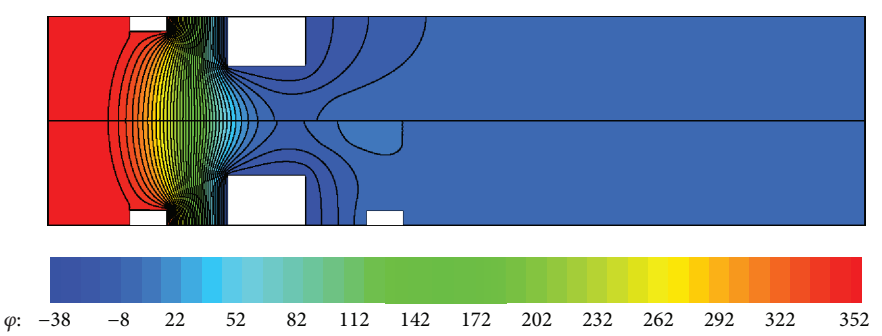

Figure 6: Potential distribution ($n_0 = 2.0$).

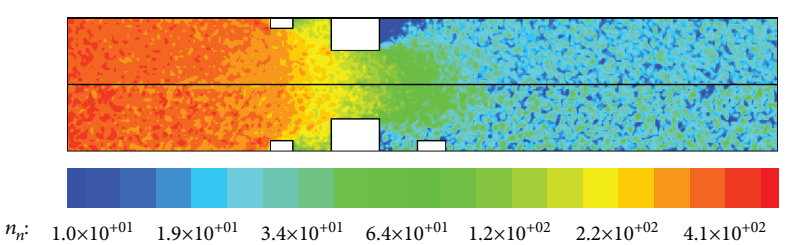

Figure 7: Number density distribution of neutral atoms.

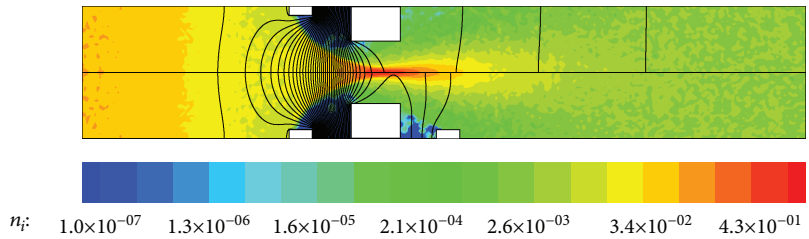

Figure 8: Beam distribution with CEX ($n_0 = 0.075$).

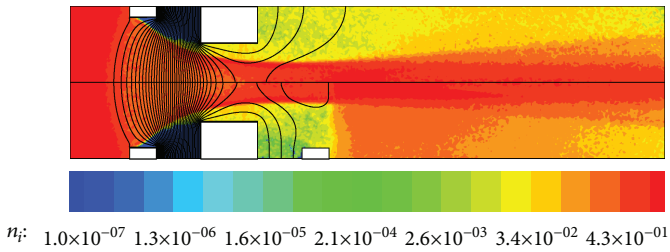

Figure 9: Beam distribution without CEX ($n_0 = 2.0$).

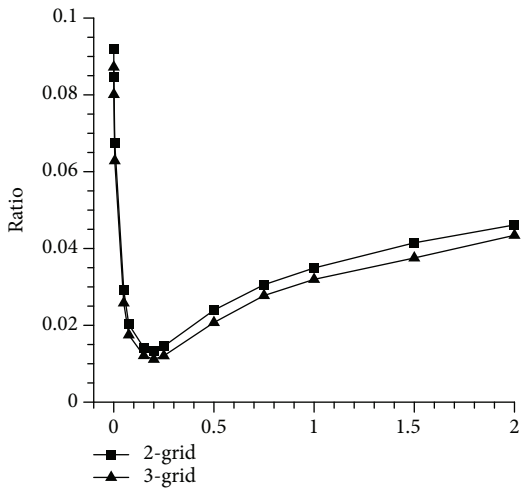

Figure 10: The ratio of the impingement current of the accelerator grid to the beam current.

grid aperture barrel, the number of CEX ions is extremely rare. However, the CEX ions from the extraction (center) region is dominant, so the CEX ions from the extraction (center) region are the main cause of the accelerator grid Barrel erosion. In the 3-grid optics, the impingement current of the accelerator grid caused by the CEX ion from the extraction (center) region is almost the same with that of the 2-grid optics, while the CEX impingement current of the accelerator grid from downstream is also significantly increased. However, the degree of the increase is lower than that at $n_0 = 0.075$ and $n_0 = 0.2$. Therefore, after adding the decelerator grid, at $n_0 = 0.75$, the accelerator Barrel erosion also increased significantly, but the degree of increase is lower than that at $n_0 = 0.075$ and $n_0 = 0.2$.

At $n_0 = 2.0$, in the 2-grid optics, the CEX ion from the upstream disappeared and the impingement current of the accelerator grid caused by the CEX ion from the extraction (center) region is the largest, which is the main factor causing the accelerator grid Barrel erosion. In the 3-grid optics, CEX ions from the upstream also disappear, and the CEX ion impingement current of the accelerator grid from the extraction (center) region is the same as that of the 2-grid optics as well. Hence, the CEX ions from the extraction (center) region are also the main factor causing the accelerator gird Barrel erosion in the 3-grid optics. But it is worth noting that the CEX impingement current of the accelerator grid from downstream decreases slightly. Therefore, after adding the decelerator grid, there is no change in the erosion of the accelerator grid aperture barrel at $n_0 = 2.0$.

3.3. Effect of the Decelerator Grid on the Downstream CEX Ions. Due to the little difference of the distribution of neutral atoms and the distribution of beam ions between the 2-grid and 3-grid optics, the generation rate of the CEX ions of these two optics will be basically the same. On the other hand, since the decelerator grid only affects the downstream potential of the optics system, the focusing state of CEX ions will be the same. Therefore, the decelerator grid will have little effect on the CEX ions from the upstream and extraction (center) regions. However, the CEX ions from the downstream will be affected significantly. Hence, in this section, the effect of the decelerator grid on the downstream CEX ions is mainly discussed.

As stated before, at $n_0 = 0.075$, $n_0 = 0.2$, and $n_0 = 0.75$, the number of CEX ions from the downstream causing the accelerator grid Barrel erosion is increased, while it decreases at $n_0 = 2.0$. It indicates that the effect of the decelerator grid on the downstream CEX ions varies with the upstream plasma number density.

Figures 11 and 12 illustrate the potential distributions of the downstream surface of the accelerator grid in the 2-grid

Table 5: Average erosion rate of 2-grid and 3-grid optical systems (unit: m/1000 h).

Density	Barrel erosion rate (by CEX ions)			Pit and Groove erosion rate(by CEX ions)		
	2-grid	3-grid	Reduction (%)	2-grid	3-grid	Reduction (%)
0.075	3.5215×10^{-6}	5.6802×10^{-6}	-61.36	2.0677×10^{-6}	4.7612×10^{-8}	97.70
0.2	9.5643×10^{-6}	1.4798×10^{-5}	-52.72	1.4160×10^{-5}	2.3608×10^{-7}	98.34
0.75	6.1906×10^{-5}	7.5255×10^{-5}	-21.45	1.2571×10^{-4}	7.1011×10^{-6}	94.37
2.0	7.2361×10^{-4}	7.2432×10^{-4}	0.00	7.2439×10^{-4}	4.4016×10^{-5}	93.92

Table 6: CEX impingement current of the accelerator grid J and mean incident energy $\bar{E}$ from different regions at $n_0 = 0.075$.

Generation region	J (A)		$\bar{E}$ (eV)	
	2-grid	3-grid	2-grid	3-grid
Upstream	1.4322×10^{-8}	1.4051×10^{-8}	1934.0	1934.7
Extraction (center)	4.1011×10^{-10}	4.3215×10^{-10}	211.81	196.66
Extraction (edge)	3.3325×10^{-10}	2.9008×10^{-10}	189.37	194.11
Downstream	4.0912×10^{-9}	3.7127×10^{-8}	197.30	178.32
Total	1.8488×10^{-8}	5.1900×10^{-8}	1461.9	993.53

Table 7: CEX impingement current of the accelerator grid J and mean incident energy $\bar{E}$ from different regions at $n_0 = 0.2$.

Generation region	J (A)		$\bar{E}$ (eV)	
	2-grid	3-grid	2-grid	3-grid
Upstream	4.3281×10^{-8}	4.2755×10^{-8}	1945.9	1946.0
Extraction (center)	4.1025×10^{-9}	3.9469×10^{-9}	240.60	235.63
Extraction (edge)	4.0877×10^{-9}	7.8354×10^{-10}	153.72	206.17
Downstream	1.0105×10^{-8}	1.2563×10^{-7}	273.11	174.62
Total	6.1576×10^{-8}	1.7311×10^{-7}	1428.8	651.73

Table 8: CEX impingement current of the accelerator grid J and mean incident energy $\bar{E}$ from different regions at $n_0 = 0.75$.

Generation region	J (A)		$\bar{E}$ (eV)	
	2-grid	3-grid	2-grid	3-grid
Upstream	5.2321×10^{-11}	5.0160×10^{-11}	1944.1	1946.8
Extraction (center)	8.2956×10^{-7}	8.2010×10^{-7}	344.44	300.53
Extraction (edge)	1.2231×10^{-8}	6.1069×10^{-9}	211.76	222.22
Downstream	1.2976×10^{-7}	3.0766×10^{-7}	128.46	172.18
Total	9.7156×10^{-7}	1.1284×10^{-6}	307.83	257.38

Table 9: CEX impingement current of the accelerator grid J and mean incident energy $\bar{E}$ from different regions at $n_0 = 2.0$.

Generation region	J (A)		$\bar{E}$ (eV)	
	2-grid	3-grid	2-grid	3-grid
Upstream	0.0000	0.0000	0.0000	0.0000
Extraction (center)	6.3902×10^{-6}	6.3681×10^{-6}	491.41	486.88
Extraction (edge)	2.1765×10^{-8}	1.0967×10^{-8}	234.02	239.43
Downstream	8.8207×10^{-7}	8.1120×10^{-7}	141.78	153.10
Total	7.2940×10^{-6}	7.1903×10^{-6}	450.25	442.02

optics and those of the decelerator grid in the 3-grid optics. It can be seen that the potential inside the accelerator grid hole in the 2-grid optics is higher than the accelerator grid potential. Hence, only some of the CEX ions produced in the downstream region can flow back into the hole. Most of the downstream CEX ions will be affected by the negative potential of the accelerator grid and flow back to the downstream surface of the accelerator grid. The potential distributions of the downstream surface of the decelerator grid in the 3-grid optics varied with the working conditions. The potential in the decelerator grid hole is smaller than that of the decelerator at

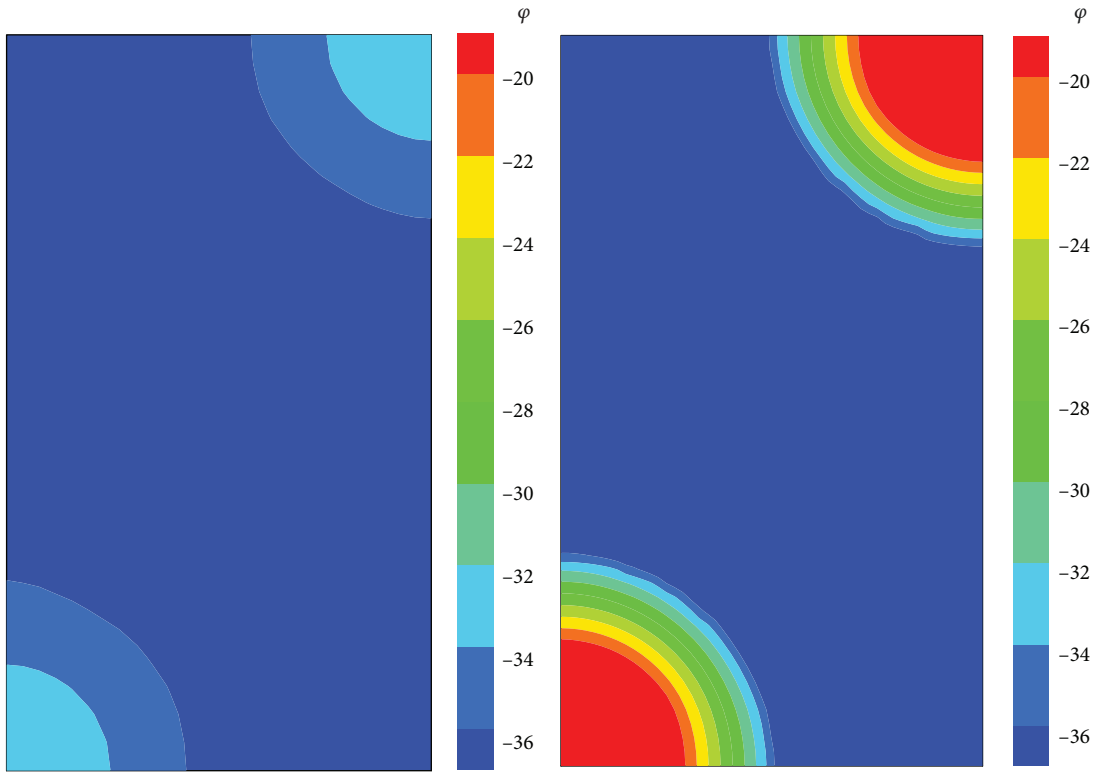

(a) $n_0 = 0.075$ (b) $n_0 = 2.0$

Figure 11: Potential distribution of the downstream surface of the accelerator grid of the 2-grid optics.

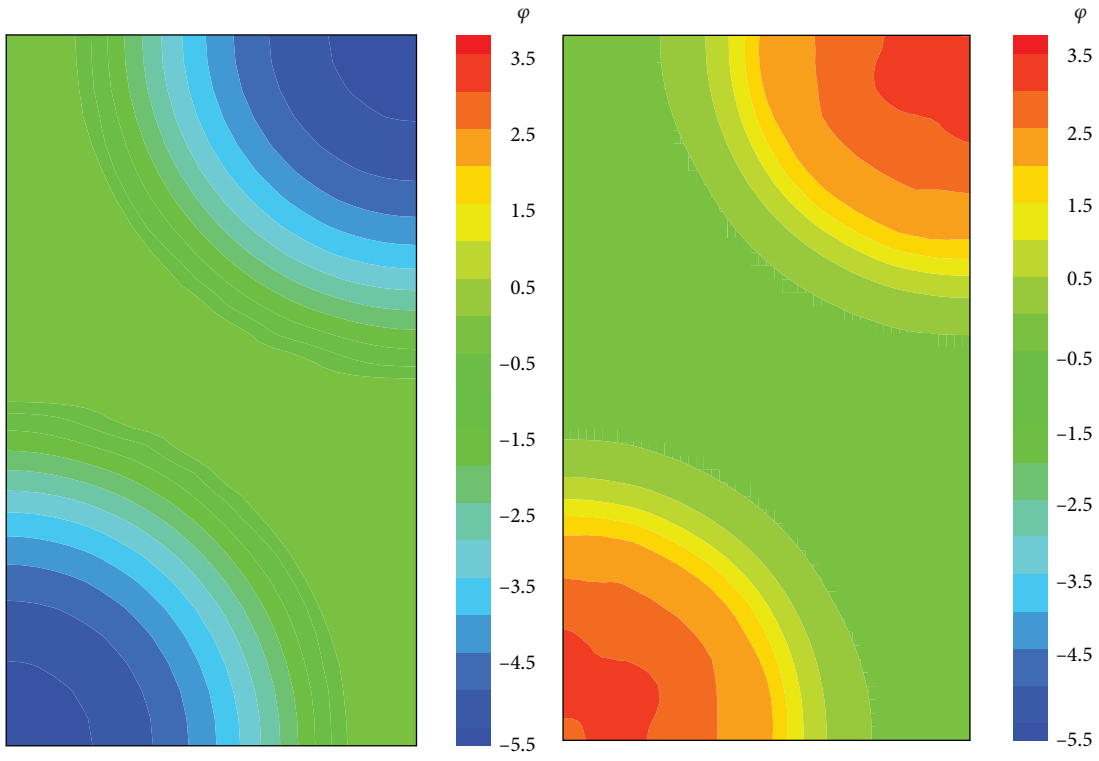

(a) $n_0 = 0.075$ (b) $n_0 = 2.0$

Figure 12: Potential distribution of the downstream surface of the decelerator grid of the 3-grid optics.

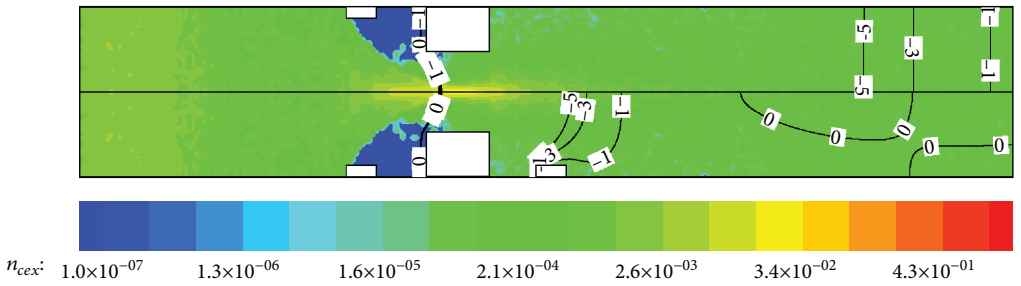

Figure 13: CEX ions and potential distribution at $n_0 = 0.075$.

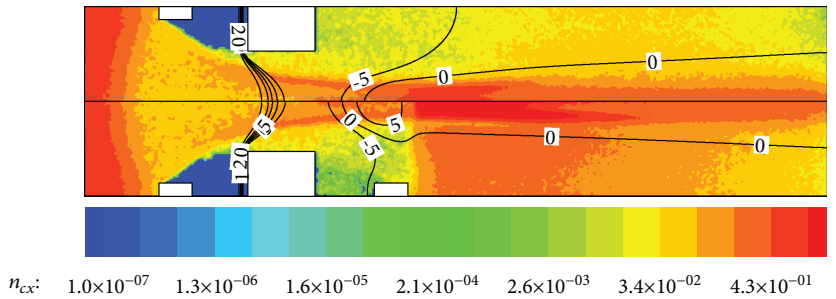

Figure 14: CEX ions and potential distribution at $n_0 = 2.0$.

$n_0 = 0.075$, while the potential in the decelerator grid hole becomes larger than the decelerator potential at $n_0 = 2.0$.

Figures 13 and 14 compare the distribution of CEX ions in the 2-grid optics and the 3-grid optics at $n_0 = 0.075$ and $n_0 = 2.0$, respectively. In the 3-grid optics, at $n_0 = 0.075$, the potential inside the decelerator grid hole is less than 0 and presents a potential structure which can reverse focus the CEX ions in the downstream. Therefore, in the 3-grid optics, the CEX ions generated from the downstream are reversely focused into the decelerator grid hole and tend to impinge on the accelerator grid aperture barrel. At $n_0 = 2.0$, the potential inside the decelerator grid hole is greater than 0. Hence, the downstream CEX ions can be blocked by the decelerator grid.

As shown in Figure 15, the potential at the hole center in the decelerator grid downstream surface becomes larger with the increase of the upstream plasma number density. When the upstream plasma number density is very small, the beam ion density is small and the space charge potential inside the hole is less than the potential of the wall. It leads to the CEX ions being heavily absorbed into the hole of the decelerator grid, which also increases the number of CEX ions flowing back into the accelerator grid hole. When the upstream plasma number density increases gradually, the decelerator grid potential becomes less than that inside the hole. Most of the reflux CEX ions in the downstream tend to impinge on the decelerator grid, so the decelerator grid can effectively block the CEX ions from the downstream.

Table 10 shows the downstream CEX ion impingement current on the accelerator grid and the reduction ratio of the 3-grid system compared with those of the 2-grid system. As far as the total CEX ion impingement current on the accelerator grid is concerned, after adding the decelerator

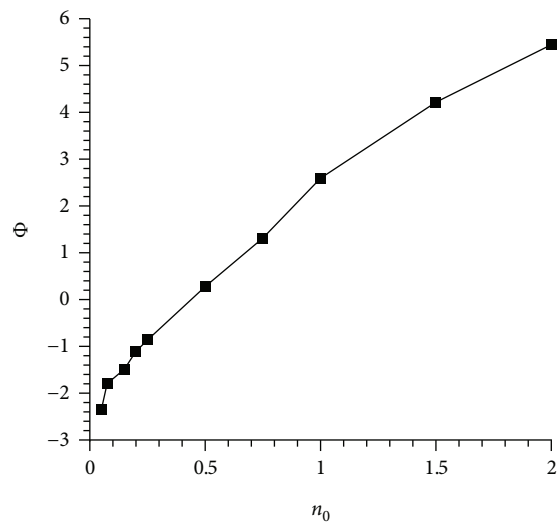

Figure 15: The variation curve of the decelerator grid downstream hole center potential with the upstream plasma number density in the 3-grid optical system.

grid, the downstream CEX ion impingement current on the accelerator grid decreases in these four different upstream plasma number densities. However, the CEX ion impingement current of the accelerator grid aperture barrel and the downstream surface does not decrease at the same time. At $n_0 = 0.075$, $n_0 = 0.2$, and $n_0 = 0.75$, the CEX ion impingement current on the accelerator grid aperture barrel increases significantly, while the accelerator grid CEX ion impingement current on the downstream surface decreases significantly. At $n_0 = 2.0$, the CEX ion impingement current of the

Table 10: The downstream reflux CEX ion impingement current of the accelerator grid and the reduction ratio.

Density	Total (A)			Aperture barrel (A)			Downstream surface (A)		
	2-grid	3-grid	Reduction (%)	2-grid	3-grid	Reduction (%)	2-grid	3-grid	Reduction (%)
0.075	7.6×10^{-8}	4.3×10^{-8}	43.4	4.1×10^{-9}	3.7×10^{-8}	-802.4	7.2×10^{-8}	6.2×10^{-9}	91.4
0.2	3.6×10^{-7}	1.7×10^{-7}	52.8	1.0×10^{-8}	1.2×10^{-7}	-1100.0	3.5×10^{-7}	5.4×10^{-8}	84.6
0.75	2.8×10^{-6}	1.1×10^{-6}	60.7	1.3×10^{-7}	3.1×10^{-7}	-138.5	2.7×10^{-6}	8.1×10^{-7}	70.0
2.0	1.5×10^{-5}	7.2×10^{-6}	52.0	8.8×10^{-7}	8.1×10^{-7}	8.0	1.4×10^{-5}	6.4×10^{-6}	54.3

Table 11: Proportion of downstream reflux CEX ions impinging on the aperture barrel and the downstream surface.

Density	Aperture barrel		Downstream surface	
	2-grid	3-grid	2-grid	3-grid
0.075	5.4%	85.6%	94.7%	14.4%
0.2	2.8%	69.2%	97.2%	30.8%
0.75	4.6%	27.2%	96.4%	72.8%
2.0	5.9%	11.1%	93.3%	88.9%

accelerator grid aperture barrel is slightly reduced, while the accelerator grid CEX ion impingement current on the downstream surface is still significantly reduced, but the reduction ratio declined compared with the other three working conditions. This result shows that, after adding the decelerator grid, the reduction ratio of the CEX ion impingent current of the accelerator grid aperture barrel and the downstream surface will change simultaneously with the variation of the operating conditions. Hence, the decelerator grid will affect the reflux CEX ions that impinge on both the aperture barrel and the downstream surface of the accelerator grid.

Table 11 presents the proportion of CEX ions from the downstream that impinge on the aperture barrel and the downstream surface of the accelerator grid, for both the 2-grid and 3-grid systems. In the 2-grid system, most of the CEX ions from the downstream hit the downstream surface of the accelerator grid, no matter the upstream plasma number density. However, for the 3-grid system, more CEX ions from the downstream hit the aperture barrel, rather than the downstream surface, with the decrease of the upstream plasma number density.

In brief, after adding the decelerator grid, the impingement current of the accelerator grid caused by CEX ions from the upstream and extraction (center) regions is basically unchanged under the over-focused and normal-focused conditions. However, when the upstream plasma number density is small, since the potential inside the decelerator grid hole is negative, most of the downstream reflux CEX ions reflow through the decelerator grid hole and impinge on the aperture barrel of the accelerator grid, causing the Barrel erosion of the accelerator grid of the 3-grid optics to increase significantly. Only when the upstream plasma number densities are large enough and the potential inside the decelerator grid hole becomes larger than the decelerator grid potential can the decelerator grid effectively block the reflux CEX ions from the downstream.

4. Summary and Conclusions

In this paper, the influence of the decelerator grid on the optical performance is investigated in detail through numerical simulations. Results indicate that the decelerator grid has little effect on the beam ions, as well as the CEX ions from the upstream and extraction (center) regions, but significantly affects the reflux CEX ions from the downstream. After adding the decelerator grid, the negative potential inside the decelerator grid hole attracts more CEX ions to impinge on the downstream surface of the accelerator grid, while the CEX ions from the upstream and extraction (center) regions leading to the Barrel erosion of the accelerator grid are basically the same, and this causes the significant increase of the erosion of the accelerator grid aperture barrel. With the increase of the upstream plasma number density, the potential inside the hole gradually increases to the level greater than the decelerator grid potential. Then, the decelerator grid begins to effectively block the reflux CEX ions in the downstream, and the accelerator grid Barrel erosion rate in the 3-grid optics is basically the same as that of the 2-grid optics.

Data Availability

The authors confirm that the data supporting the findings of this study are available within the article.

Conflicts of Interest

The authors declare that they have no conflicts of interest.

Authors' Contributions

Chang Lu and Yide Zhao contributed equally to this work.

Acknowledgments

This work was supported by the Open Fund for the National Key Laboratory of Science and Technology on Vacuum Technology and Physics under Contract no. ZWK1703 and the program of the Shenzhen Technology Projects (JCYJ20160817172025986, JCYJ20160226201347750). This work was also supported by the Key Laboratory of Robotics and Intelligent Equipment of Guangdong Regular Institutions of Higher Education (Grant No. 2017KSYS009). The authors thank the sponsors of the 2nd Asia-Pacific Conference on Plasma Physics for providing an opportunity to exchange and discuss the ideas in this paper.

References

[1] Q. Zhang, X. Peng, and D. Keefer, "Particle simulation of grid erosion for a three-grid ion thruster," in *IEPC Paper*, pp. 93–178, Seattle, WA, USA, 1993.

[2] R. E. Wirz, J. R. Anderson, D. M. Goebel, and I. Katz, "Decel grid effects on ion thruster grid erosion," *IEEE Transactions on Plasma Science*, vol. 36, no. 5, pp. 2122–2129, 2008.

[3] G. Meadows and B. Free, "Effect of a decel electrode on primary and charge-exchange ion trajectories," in *11th Electric Propulsion Conference*, p. 427, New Orleans, LA, USA, March 1975.

[4] J. Wang, J. Polk, J. Brophy, and I. Katz, "Three-dimensional particle simulations of ion-optics plasma flow and grid erosion," *Journal of Propulsion and Power*, vol. 19, no. 6, pp. 1192–1199, 2003.

[5] J. Polk, J. Brophy, and J. Anderson, "Numerical simulations of ion thruster accelerator grid erosion," in *38th AIAA/ASME/-SAE/ASEE Joint Propulsion Conference & Exhibit*, pp. 4261–4275, Indianapolis, Indiana, July 2002.

[6] S. Anbang, M. Genwang, Y. Juan, X. Guangqing, C. Maolin, and H. Chao, "Particle simulation of three-grid ECR ion thruster optics and erosion prediction," *Plasma Science and Technology*, vol. 12, no. 2, pp. 240–247, 2010.

[7] J. J. Wang, Y. Cao, R. Kafafy, R. Martinez, and J. Williams, "Numerical and experimental investigations of crossover ion impingement for subscale ion optics," *Journal of Propulsion and Power*, vol. 24, no. 3, pp. 562–570, 2008.

[8] R. Kafafy and J. Wang, "Whole ion optics gridlet simulations using a hybrid-grid immersed-finite-element particle-in-cell code," *Journal of Propulsion and Power*, vol. 23, no. 1, pp. 59–68, 2007.

[9] T. Lin and J. Wang, "An immersed finite element electric field solver for ion optics modeling," in *Proceedings of AIAA Joint Propulsion Conference*, pp. 2002–4263, Indianapolis, IN, USA, 2002.

[10] R. Kafafy, T. Lin, and J. Wang, "3-dimensional ion optics simulations using an IFE–PIC code," in *AIAA Paper*, pp. 3–5164, Huntsville, AL, USA, 2003.

[11] R. Kafafy and J. Wang, "Whole ion optics simulations of a subscale gridlet using a hybrid-grid IFE-PIC code," in *40th AIAA/ASME/SAE/ASEE Joint Propulsion Conference and Exhibit*, pp. 3783–3783, Fort Lauderdale, FL, USA, July 2004.

[12] H. Cao, Y. Chu, E. Wang, Y. Cao, G. Xia, and Z. Zhang, "Numerical simulation study on barrel erosion of ion thruster accelerator grid," *Journal of Propulsion and Power*, vol. 31, no. 6, pp. 1785–1792, 2015.

[13] H. Jian, Y. Chu, H. Cao, Y. Cao, X. He, and G. Xia, "Three-dimensional IFE-PIC numerical simulation of background pressure's effect on accelerator grid impingement current for ion optics," *Vacuum*, vol. 116, pp. 130–138, 2015.

[14] C. Lu, T. P. Zhang, P. Qiu, J. J. Chen, Y. Cao, and L. Zheng, "Barrel erosion of ion thruster accelerator grid under different operating conditions," *IEEE Transactions on Plasma Science*, vol. 46, no. 12, pp. 4065–4077, 2018.

[15] R. Killinger, H. Bassner, J. Mueller, and R. Kukies, "RITA ion propulsion for ARTEMIS lifetime test results," in *36th AIAA/ASME/SAE/ASEE Joint Propulsion Conference and Exhibit*, pp. 3273–3282, Las Vegas, NV, USA, July 2000.

[16] H. J. Leiter, R. Killinger, H. Bassner, J. Mueller, R. Kukies, and T. Froehlich, "Development and performance of the advanced radio frequency ion thruster RIT-XT," in *28th International Electric Propulsion Conference (IEPC 2003)*, pp. 115–124, Toulouse, France, 2003.

[17] H. Bassner, R. Bond, V. Thompson, and K. Groh, "The development of the ESA-XX ion thruster," in *International Electric Propulsion Conference*, pp. 120–127, Cleveland, OH, USA, 1997.

[18] K. Groh, P. Fahrenbach, and H. Loeb, "Primary ion thruster ESA-XX for interplanetary missions," in *31st Joint Propulsion Conference and Exhibit*, pp. 2520–2529, San Diego, CA, USA, July 1995.